Available online at www.sciencedirect.com
ScienceDirect
JOURNAL OF IRON AND STEEL RESEARCH, INTERNATIONAL. 2013, 20(11): 57-66

Elasto-Plastic Test of Q235 Steel Bending Beam With Cracking Resistance

WANG Li-min[1], FENG Ying[1], CHEN Fan-xiu[1], WANG Hai-ying[2], WANG Dong-xu[1]
(1. Science School, Qingdao Technological University, Qingdao 266033, Shandong, China;
2. Institute of Mechanics, Chinese Academy of Sciences, Beijing 100190, China)

Abstract: More than 30 bending beams with rectangular cross-section and different thicknesses and heights were prepared from Q235 steel. The specimen dimensions were about 240 mm (length) ×60 mm (height) ×70 mm (thickness). Flaws were cut along its middle line with a wire cutter, with lengths ranging from 6 to 35 mm. Each specimen was tested with three-point bend loading, and a process curve was obtained between load and the displacement of the loading point, in order to analyze the fracture process when opening the crack. A deformation near the prefabricated crack was observed in the testing period, and the variation of the fracture characteristic parameters was analyzed for different sizes. For a comprehensive understanding of carbon steel fracture resistance behavior, its elasticity and plasticity were established by determining its Young's modulus and Poisson's ratio with an optical strain gauge. This gauge was also used for the loading process test. It was found that the fracture toughness varied with the dimensions, and the toughness of the elastic limit loading was almost constant. Using the relationship of crack resistance stress intensity factor and fracture criterion, the bearing capacity of the material structure could be estimated, which shows a good agreement with the experimental test data.

Key words: elasto-plastic property; fracture toughness; elastic limit loading; bearing capacity; cracking resistance; Q235 steel; bending beam

For evaluating the strength and bearing capacity of a material structure containing defects at normal temperature, fracture mechanics is an effective tool for quantitative analysis, although the failure process and fracture surface characteristics differ greatly between brittle materials and tough materials. The stress intensity factor (SIF) and energy release rate are important indices in this area. For tough elasto-plastic materials, such as alloys and carbon steel, the values of the J-integral, crack opening displacement (COD), and crack tip opening angle (CTOA) are important parameters for the description of the cracked body status[1]. Mesoscopic research has identified different defects, including voids or cracks in the material, and their increase and spread. For the dislocation and sliding in metal and their large deformations, tensor analysis is an effective method of study[2-3]. The strain gradient can be used to analyze the complex fields of force and deformation near a crack tip[4]. The toughness and brittleness can be reproduced in the same material. For instance, a material may become brittle when its temperature is reduced to some extreme level, or it may be subjected to brittle fracture when its crack tip tri-axial tension stress is increased to some value[5]. The mechanical behavior of cracking materials has given rise to many research models, such as the asymptotic field analysis of cohesive crack, the double-K model, and the size-effect law[6-8]. Regarding the cohesive crack problem, the open displacement of a virtual crack and its stress distribution were obtained by means of an integral equation and a variational principle[9]. Regardless, the observation and measurement of deformation in a cracked material structure, especially at the crack tip, are indispensable for failure analysis, and they also provide the theoretical analysis basis for study[10].

For a rectangular cross-section bending beam of Q235 steel with a prefabricated crack, the breaking process was studied using electronic instruments and optical measurement devices. Several specimens with different prefabricated crack lengths were tested.

Foundation Item: Item Sponsored by National Natural Science Foundation of China (51008166, 11172311, 10272068)
Biography: WANG Li-min(1962—), Male, Doctor, Professor; **E-mail**: wanglimin@qtech.edu.cn; **Received Date**: November 15, 2011

The Young's modulus and Poisson's ratio of the material were also calculated through strain gauge measurement. The deformation field at the crack front was investigated for determining the variation of fracture parameters with structure size. Based on the calculation of the crack resistance SIF and fracture criterion, the bearing capacity of the bending beams with crack could be obtained.

1 Cracking Process Test on Three-Point Bending Beam

1.1 Specimen geometry and loading curve analysis

Carbon steel was precut into more than 30 pieces of beam specimens of different sizes in order to test the loading process. The overall length of the specimens L was 300 mm, their height h was 60 or 65 mm, and their thickness b was 30, 40, 50, 60, or 70 mm. The lengths of the prefabricated crack a were 6, 12, 18, 25, or 35 mm, and the crack width was about 1 mm. A notch was precut in the middle of the bending beam tension side, so that an opening mode crack (type-I) was formed in accordance with the laws of fracture mechanics. The span of each experimental beam was four times the height for each bending specimen, that is $s=4\cdot h$. Each specimen size and experimental measured peak load are listed in Table 1, where c is the specimen's ligament length; P is its maximum load; $K_{\mathrm{I}}^{\mathrm{e}}$ and CODe are the SIF and COD of the elastic limit load, respectively; and $K_{\mathrm{I}}^{\mathrm{u}}$ is the SIF value of specimen for unstable fracture. Furthermore, the symbols in the first column in Table 1 are consistent with these above symbols, the number following the symbol indicating its value. For example, "h60b50a25" indicates a specimen with height of 60 mm, thickness of 50 mm, length of prefabricated crack of 25 mm, and the span between two loading points $s=240$ mm. From the data in Table 1, it can be shown that the bearing capacity of the specimen is higher when the crack is shorter or the thickness is larger.

Fig. 1 shows the relationship curves of the load to the displacement of the corresponding loading point for ten typical specimens. All specimens had the same height of $h=60$ mm and the same span of $s=240$ mm. In Fig. 1 (a), the curve of load to displacement is shown for prefabricated crack lengths of 12, 18, 25, and 35 mm, for a constant thickness of $b=60$ mm. Obviously, both the bearing capacity and deformation of the specimens increased with larger ligament. Also, the initial slopes of the elastic stage and the plastic stage both increased for longer ligament.

Table 1 Experimental data of steel specimen and its fracture parameters

Specimen	c/mm	P/kN	$K_{\mathrm{I}}^{\mathrm{e}}$/(MPa·m$^{1/2}$)	CODe/mm	$K_{\mathrm{I}}^{\mathrm{u}}$/(MPa·m$^{1/2}$)
h60b30a18	42	130.0	/	—	107.6
h60b30a18	42	126.0	/	—	104.3
h60b30a35	25	46.6	/	—	89.8
h60b30a35	25	49.3	/	—	95
h60b40a18	42	129.0	55.42	0.021 5	80.5
h60b40a25	35	91.7	56.30	0.010 7	77.7
h60b40a35	25	53.7	54.33	0.007 3	77.6
h60b50a18	42	189.0	57.14	0.006 8	93.9
h60b50a18	42	172.8	56.99	0.011 9	85.9
h60b50a25	35	131.0	54.24	0.007 1	89.3
h60b50a35	25	76.3	52.04	0.006 0	88.2
h60b60a12	48	320.0	58.35	0.016 0	102.3
h60b60a12	48	328.0	53.95	0.016 5	104.9
h60b60a18	42	236.0	53.82	0.009 7	97.7
h60b60a18	42	247.0	57.29	0.009 4	102.0
h60b60a25	35	183.0	56.06	0.009 6	102.0
h60b60a25	35	186.3	55.31	0.008 1	103.4
h60b60a35	25	101.0	51.16	0.007 1	97.3
h60b60a35	25	102.5	51.50	0.008 1	98.8
h60b70a06	54	492.0	/	—	97.2
h60b70a12	48	398.0	/	0.010 4	109.0
h60b70a12	48	419.0	/	—	115.0
h60b70a18	42	298.0	56.65	—	105.7
h60b70a25	35	218.0	56.67	0.005 6	105.6
h60b70a35	25	121.5	52.55	0.004 8	100.3
h65b30a06	59	240.3	/	—	103.0
h65b30a12	53	149.3	/	—	87.9
h65b40a12	53	188.8	56.24	—	83.4
h65b50a06	59	610.0	/	—	156.5
h65b50a06	59	596.9	/	—	153.2

In Fig. 1 (b), the length of the prefabricated crack of the specimens is 35 mm, and the thicknesses are 30, 40, 50, 60, and 70 mm. As the graph shows, the peak load became larger with the increase of the specimen thickness. The slope changes of elastic and plastic stages are not too significant. But the specimen with thickness of 30 mm demonstrated unstable brittle fracture, and almost no plastic deformation.

In Fig. 1 (c), it is shown that the specimen h60b70a18 was loaded to the stage of local plastic deformation, and then it was slowly unloaded and strengthened to a certain point of loading again. The parallel curves of reloading and unloading can be obtained by loading and unloading repeatedly. It can be observed that the relation of displacement to reloading still follows the original line of the initial elastic stage for the specimen, and the three curves of unloading are almost parallel to the curve of elastic stage. So the Q235 steel beam with a crack also obeys

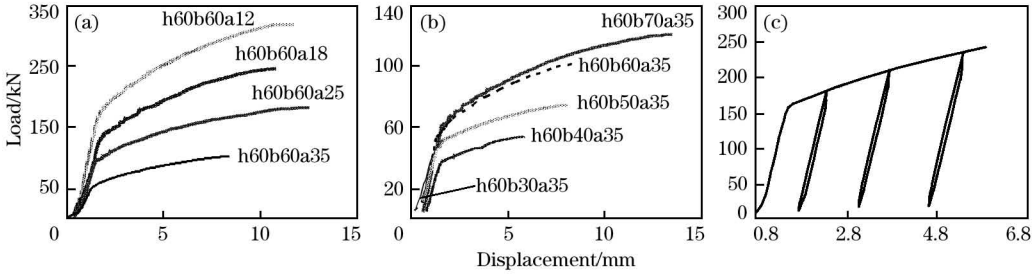

(a) Load-displacement curves for different prefabricated crack lengths; (b) Load-displacement curves for different thicknesses; (c) Unloading appearing in specimen h60b70a18.

Fig. 1 Relation of load to displacement of loading point for different specimens

"unloading law" of a structure without a crack.

From Fig. 1 (a) and (b), it should be noted that the curves of these specimens have a long plastic stage, except for specimen h60b30a35. Without much plastic deformation, as the specimen with thickness of 30 mm shows brittle fracture, a possible reason is that the beam thickness does not meet the plane strain condition.

1.2 Ligament test of breaking process and opening displacement near crack tip

In order to test the deformation about a crack, a few strain gauges with size of 20 mm×3 mm were connected with the ligament area of the prefabricated crack on a specimen. Both edges of the strain gauge were stuck to the specimen, to avoid premature detachment of the gauge. Readings from the gauge were taken with the slow loading of experimental machine. As shown in Fig. 2, the curves show the opening displacement changes of crack ligament with loading, and the displacement distribution under different load for two specimens. For the specimen h65b50a06 in Fig. 2 (a) and (b), the strain gauges A to E were located at distances from prefabricated crack tip of 2.5, 12.5, 24.5, 36.5, and 49 mm, respectively. For Fig. 2 (c) and (d), the strain gauges A, B, and C of specimen h60b60a25 indicated their distances from crack tip to be 2.5, 16.5, and 30.5 mm,

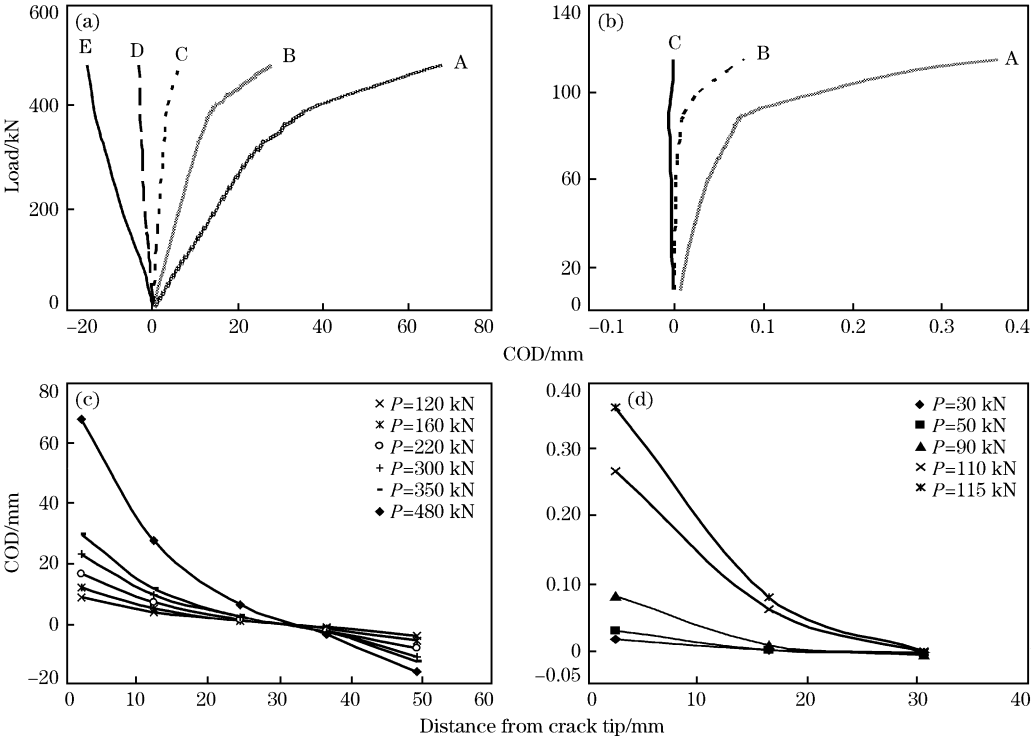

(a) Load-COD curves of specimen h65b50a06; (b) Load-COD curves of specimen h60b60a25; (c) COD distribution along cohesive crack part for specimen h60b50a06; (d) COD distribution along cohesive crack part for specimen h60b60a25.

Fig. 2 COD distribution of two specimens with different load

respectively. From those curves, it can be shown that the position with less distance from the crack tip has bigger deformation. If the initial linear line is the elastic stage character of material, Fig. 2 (a) shows that when the local material under strain gauge A first reached plastic state the load was about 320 kN; the positions at which strain gauges B and C indicated plastic state, the load was about 390 and 410 kN, respectively. From Fig. 2 (c), the development trend of the plastic zone can be seen to be the same as that of Fig. 2 (a). From these graphs, the strain gauge value near the loading point of the beam can be seen to be always negative. This shows that there is a so-called neutral layer in the bending beam loaded at three points. From Fig. 2 (b) and (d), it can be seen that the neutral layer moves slowly away from prefabricated crack tip with gradually increasing load.

Among the curves of Fig. 1, the criterion load point can be found to distinguish the segment line of the elastic stage from that of the plastic state. As to the corresponding loading point, the strain gauge value can be converted into the so-called COD of the elastic limit load, which is denoted CTODe and expressed in Fig. 3. From the chart, it is shown that longer prefabricated crack length leads to smaller CTODe value. Similarly, increasing the bending beam thickness decreases the CTODe value. So CTODe is also a parameter related to the structure geometry.

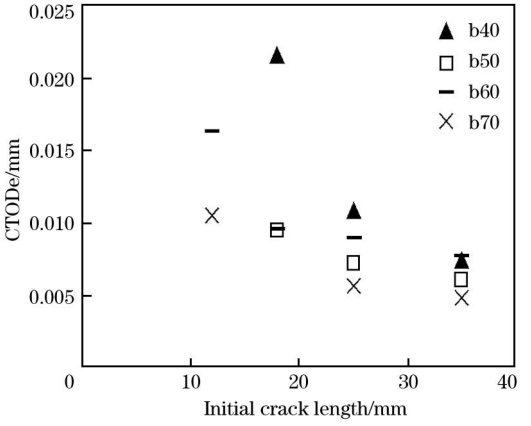

Fig. 3 Crack tip opening displacement of specimen at elastic limit loading for different thicknesses

2 Elasto-Plastic Parameters

2.1 Elastic modulus and Poisson's ratio

For the investigation of the elastic modulus and Poisson's ratio of Q235 steel, three pieces of uncracked bending beam specimen were tested with four-point loading, and their geometries are listed in Table 2. The length L and span l are 300 and 240 mm for all specimens, respectively. The distance between the two upper loading points of the specimen is 80 mm. The specimen shape and strain gauge position are shown in Fig. 4 (a). The strain gauge was used to obtain the strain measurements in vertical and horizontal directions, and the strain gauge was pasted on the geometric center of the underside of the specimen. The dimension of the strain gauge was about 5 mm×3 mm, its resistance is 120 Ω, and its sensitivity coefficient is about 2.1%. In Fig. 4 (b), the curve of stress to strain is shown for the measurement of specimen h65b40. The elastic modulus can be obtained through the strain value and the calculated stress, i.e. $E=\sigma/\varepsilon$, where ε is the strain value along the longitudinal line of specimen read from the instrument, and σ is its stress. For a specimen of rectangle cross-section beam with four-point loading, the maximum normal stress of bending beam is near the middle of specimen, that is:

$$\sigma=\frac{M}{W}=\frac{3P(l-s)}{2bh^2} \tag{1}$$

where P is the load value for the elastic stage, and $l-s=160$ mm. The Poisson's ratio can also be calculated as follows:

$$\upsilon=\frac{\varepsilon'}{\varepsilon} \tag{2}$$

where ε and ε' are the strains of longitudinal and transverse directions, respectively, and they can be directly obtained through the values of the strain gauges. Finally, the average experimental value is obtained through the experimental results of three specimens, as shown in Table 2. The experimental results show good agreement with the theoretical value, as the test results are in the common data range.

Table 2 Geometry of bending beam specimen and its testing elastic parameters

	h/mm	b/mm	E/GPa	υ
h65b40	65	40	203.0	0.26
h65b40	65	40	195.0	0.29
h60b60	60	60	222.0	0.28
Average	—	—	206.7	0.28

2.2 Measurement of Poisson's ratio in plastic deformation stage

The uncracked specimens h65b40 and h60b60 were tested by the bending beam with four-point loading, as shown in Fig. 4. In the plastic deformation stage of the specimen, some three groups of strain values in longitudinal and vertical directions were

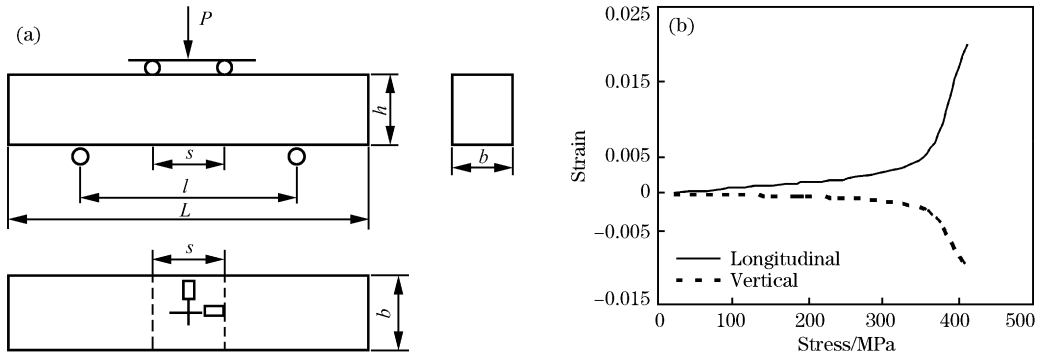

(a) Geometry of specimen and strain gauge position; (b) Stress-strain curves for two directions of specimen.

Fig. 4 Experiment about specimen h65b40

obtained for the calculation of Poisson′s ratio in plastic status. From Eqn. (2), the Poisson′s ratio of the strengthening stage of the experimental metal is calculated, and the average value is about 1/2. According to classical plastic theory, the plastic deformation of a solid is unrelated to its hydrostatic stress. The invariance of the solid volume implies its Poisson′s ratio is equal to 1/2. The test data of Q235 steel confirm that the classical plastic hypothesis is reasonable.

3 Optical Test and Electrical Measurement Reference

3.1 Optical test and electrical measurement

For digital speckle correlation measurement (DSCM), or digital images related method, the displacement and strain information is obtained directly by comparing two digital images with solid surface before and after deformation. In the experiment, a charge coupled device (CCD) camera was placed in the same horizontal position as the specimen, and the brightness and angle of the light source were adjusted to optimum, then fixed. The specimen h60b40a25 was tested by the DSCM in two dimensions. The specimen surface was firstly ground smoothly, then the central line of the speckle field was placed along the prefabricated crack line. The distance of the left and right sides to the crack line is 40 mm. Some white paint was evenly sprayed onto the selected area, in order to make imaging clear. A little black paint was then scattered in the field, for obvious speckles.

In the optical measurement experiment, the strain gauges were also pasted on the other side of the specimen, as a reference. The distances of three pieces of strain gauges to the tip of prefabricated crack are 2.5, 12.5 and 22.5 mm. The strain gauge specification is 20 mm×3 mm. The geometry of the specimen is shown in Fig. 5.

The maximum load of specimen was 91.7 kN when the loading changed from zero to the final loading of its fracture. In the elastic stage, speckle images were collected at intervals of 10 kN. The loading interval of acquisition image was about 5 kN while plastic deformation was appearing near the crack tip. A series of speckle images are selected of the initial

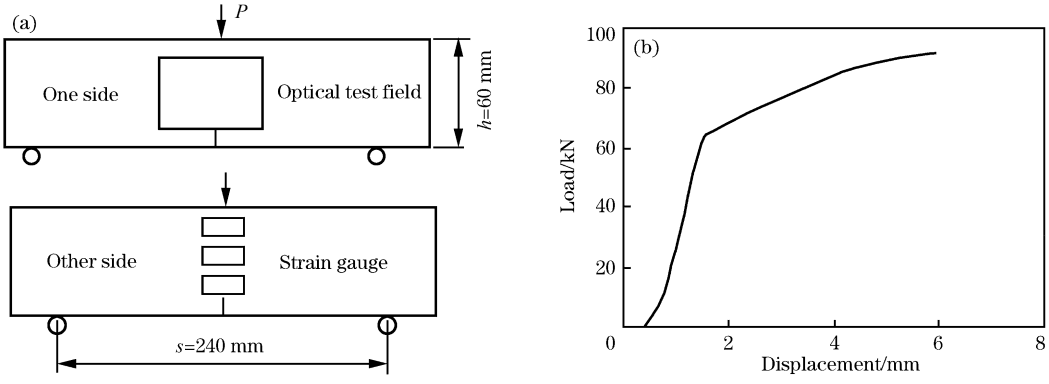

(a) Positions of optical test and strain gauge; (b) Curves of load-displacement relation for the specimen.

Fig. 5 Optical and electrical measurement on specimen h60b40a25

state of the crack, the crack extension, and the final fracture, to express the fracture process of a specimen. Fig. 6 shows images near the prefabricated crack for loads of 0, 67, 80, and 91.7 kN. From the curve of the loading and its displacement in Fig. 5 (b), the specific load of the curve inflection point is 65 kN nearly. By inspection, an obvious deformation near the crack can be seen in Fig. 6 (b), showing that the observation results are in agreement with electrical measurement.

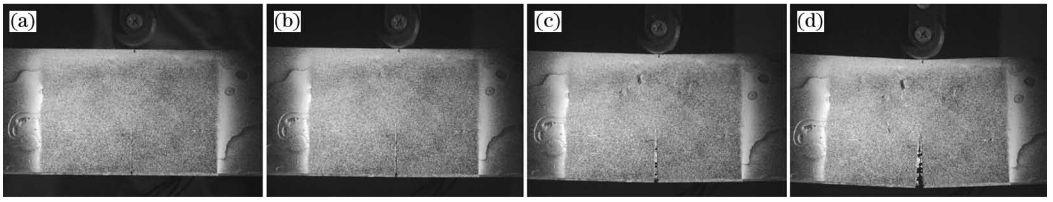

(a) 0 kN; (b) 67 kN; (c) 80 kN; (d) 91.7 kN.

Fig. 6 Cracking images of specimen h60b40a25 under different loads

3.2 Analysis of optical test results

The data from the images obtained were imported into the computer software for processing. In the experiment, the analysis field of optical measurement is a selection square, with its center at the tip of the prefabricated crack. There are 18 pixels below the crack tip, 382 pixels above the point, and about 295 pixels on both sides. Referring to Fig. 5 (b), the analysis data are selected at a load of 30 kN in the elastic stage and a load of 60 kN close to the plastic deformation stage. The data at a load of 70 kN are regarded as relating to the strengthening plastic stage of the specimen, and the data at 90 kN are close to its breaking phase. As shown in Fig. 7, the x- and y-axes in the speckle field indicate the horizontal direction and vertical direction, respectively. The third direction in Fig. 7 indicates the displacement values of the observation area (either direction). Fig. 7 (a), (b), (c), and (d) correspond to horizontal displacement distribution for the loads of 30, 50, 70, and 90 kN, while Fig. 7 (e), (f), (g), and (h) correspond to the displacement field in the vertical direction for the same series load, respectively. The right displacement is positive for the horizontal direction (x-axis), and the left is negative. As to the vertical displacement (y-axis direction), the displacement of the "up" direction is positive, and the "down" is negative.

From Fig. 7 (a) to (d), it can be seen that the horizontal displacement varies with increasing load. Obviously, displacement difference exists near the crack tip, and the displacement of crack right flank is

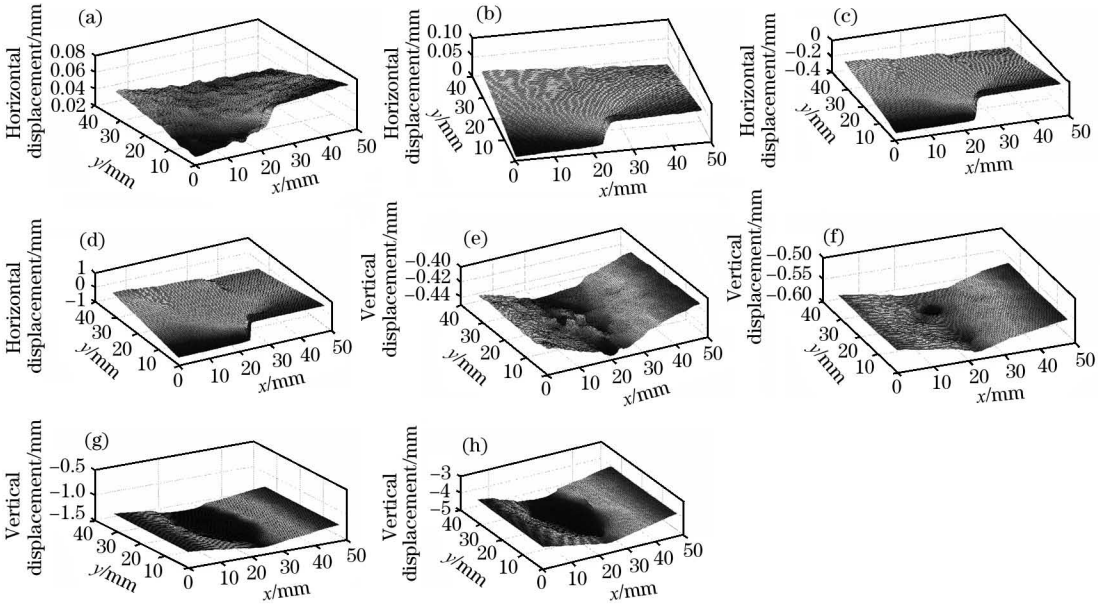

(a), (e) 30 kN; (b), (f) 50 kN; (c), (g) 70 kN; (d), (h) 90 kN.

Fig. 7 Specimen displacement field near crack tip with different loads in horizontal and vertical directions

obviously higher than that of the left. As displacement jumps exist at both sides of the crack line, it is clear that displacement of the crack right flank during loading tends to the right, and the left side displacement is to the left. Fig. 7 (a) and (b) show the elastic stage of specimen. Because the displacement of specimen is greater than zero, it shows there is a rigid displacement to the right. In Fig. 7 (c) and (d), it can be seen that the location material of specimen had entered plastic status, the displacement difference near crack is more obvious, and negative displacement had also appeared. The displacement features of both flanks of the crack are more obvious, and the left flank is displaced to the left. Regarding Fig. 7 (b) and (d), it can be seen that the deformation is very obvious for the relative opening displacement of the prefabricated crack from 0.07 to 1.2 mm as the load increased from 50 to 90 kN.

As to the vertical displacement shown in Fig. 7 (e) to (h) under different loads, Fig. 7 (e) and (f) are for the elastic state, and Fig. 7 (g) and (h) are of plastic deformation. The specimen displacement of area about the center line shows as down sag, or like the character "V". The down displacement is very obvious for 0.46 to 1.0 mm when the load increases from 30 to 70 kN. Of course, some very large displacement appears near the loading point, which seems to be due to a very big pressure load in the area of the loading point.

3.3 Contrast analysis of optical test and electrical measurement

The results of observation and tests on the opening displacement of crack tip were obtained through both electronic and optical equipments. The data for plastic deformation at a load of 70 kN were selected for analysis. For more intuitive analysis, the pixels are converted into length values, 1 pixel=0.0791361 mm. So the analysis zone is now the area with its center at the crack tip and extending down about 1.42 mm, up about 30.23 mm, and to each side by 23.35 mm. If the lower left corner of the analysis area is selected as the coordinate origin, the point of crack tip is located at about (23.35, 1.42) in the coordinate system. For the electronic measurement, the coverage zone of the test strain gauge near the crack tip is more than 20 mm×3 mm. For the optically measured side, the zone is the area with center about (23.35, 2.92), each side 10 mm to the right and left, and at about 1.5 mm intervals up and down. As shown in Fig. 7 (c), it shows the displacement distribution of longitudinal direction for a load of 70 kN. The strain gauge is therefore covering the area of large displacement or plastic deformation.

During the electronic measurement, the value of COD can be directly obtained by multiplying the strain gauge data by the strain gauge length (i.e., 20 mm). Through calculation, the crack tip opening displacement is 0.162 mm by electronic measurement for the load of 70 kN, but 0.159 by the optical measurement. Comparing the two sets of data, it is concluded that error exists among the test data of optical and electronic. The strain field of crack nearby can be obtained using the optical test data of the speckle field. As shown in Fig. 8, the equivalent strain field for the optical test is for 90 kN load. From the figure, it is clear that the strain field presents a fishplate form near the crack mouth, and this feature is responsible for the plastic deformation. In the mesoscopic view, the stress strengthening or shear deformation is accompanied by dislocation and sliding, making the crack tip blunt. The morphology is approximately coincident with the plastic field of the von Mises stress criterion.

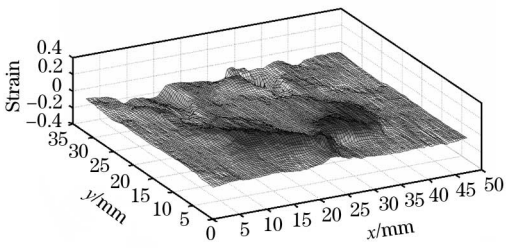

Fig. 8 Strain field of specimen h60b40a25 crack front for load of 90 kN

4 Calculation of Stress Intensity Factor and Toughness

Although the SIF is an important index to characterize the stress singularity of the medium near the crack tip, COD is also an important parameter for the characteristics of non-linear material in the fracture process. Either the plastic zone size or the crack tip opening displacement (CTOD) is closely related to SIF value. For the three-point bending beam with a notch, the SIF of the crack tip can be expressed:

$$K_{\mathrm{I}}=3Ps\sqrt{a}\{1.99-\frac{a}{h}\left(1-\frac{a}{h}\right)[2.15-3.93\frac{a}{h}+2.7\left(\frac{a}{h}\right)^2]\}/\left[2bh^2\left(1+2\frac{a}{h}\right)\left(1-\frac{a}{h}\right)^{3/2}\right] \quad (3)$$

In the loading experiment on specimens with a series of thicknesses and pre-crack lengths, the load at the elasto-plastic inflection point P_e, the elastic

limit load, and the maximum load value P for the unstable fracture of specimen can be obtained. Then, the elastic limit toughness K_I^e, or the specimen fracture toughness K_I^u can be obtained by bringing P_e or P into the above equation respectively. Here, the value of a in Eqn. (3) is replaced by the initial crack length a_0. Then, two kinds of toughness value are also included in columns 4 and 6 of Table 1. From the table data, it can be seen that the instability toughness is changing with the values of pre-crack length and beam thickness. But the toughness of the elastic limit changing little with the size of the test specimen, and K_I^e is about 55 MPa · $m^{1/2}$. Except for a few very specific specimens, the K_I^e value of the series of specimens and their error from the average value are listed in Table 3. It is seen that the absolute value of maximum deviation between any one and the mean value is less than 7%. This shows that K_I^e can be used as a material parameter, as it is generally not variable with specimen size.

If the length of the extension line of the pre-crack is the ligament, the ligament length is $c=h-a_0$. As a matter of convenience, the variation of unstable fracture toughness is expressed in terms of the ligament length changing for different thicknesses of specimen, as shown in Fig. 9. From Fig. 9 (a), it can

Table 3 Elastic limit toughness and estimated peak value of crack structure

Specimen	K^e/(MPa · $m^{1/2}$)	Error of K^e/%	Test maximum load/kN	Estimated load/kN	Relative error/%
h60b40a18	55.42	0.80	129	141.4	9.61
h60b40a25	56.30	−2.360	91.7	99.9	8.94
h60b40a35	54.33	1.218	53.73	53.5	−0.43
h60b50a18	57.14	−3.890	189	192.5	6.08
	56.99	−3.618	173		
h60b50a25	54.24	1.381	131	135.8	3.66
h60b50a35	52.04	5.381	76.3	71.9	−5.77
h60b60a12	58.35	−6.090	320	322.2	−0.56
	53.95	1.909	328		
h60b60a18	53.82	2.145	236	248.3	3.89
	57.29	−4.163	183		
h60b60a25	56.06	−1.927	183	174.9	−5.28
	55.31	−0.563	186.3		
h60b60a35	51.16	6.981	102.5	92.4	0.89
	51.50	6.363	101.0		
h60b70a06	—	/	492	505.6	2.76
h60b70a12	—	/	398	400.5	−0.87
	—	/	410		
h60a70a18	56.65	−3.000	298	308.5	3.36
h60b70a25	56.67	−3.036	218	216.9	−0.50
h60b70a35	52.55	4.454	121.5	114.3	−5.93

Note: The mean value of K^e is 54.98 MPa · $m^{1/2}$.

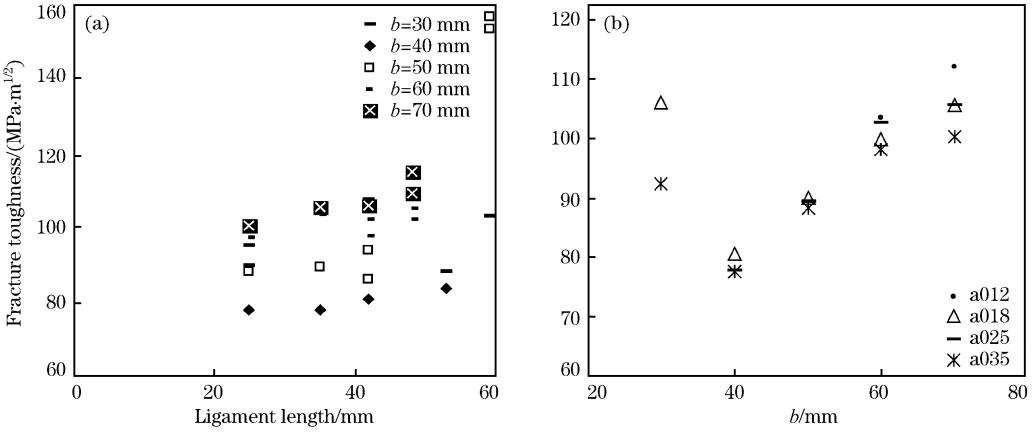

(a) For different ligament length; (b) For different thickness of specimens.

Fig. 9 Experiment toughness variation of unstable fracture

be seen that the fracture toughness is increased with its ligament length for constant thickness of specimen. Fig. 9 (b) shows that the fracture toughness becomes larger monotonically with increasing thickness for the same pre-crack length of specimen, except for the specimens of 30 mm thickness. It therefore reflects the size effect of fracture toughness for the same material.

5 Estimate Calculation for Bearing Capacity of Bending Beam With Crack

Regarding the deformation of elasto-plastic and damage of solid materials and the size effect of the fracture parameter, there are many analysis models as mentioned before. For the elasto-plastic field, the Dugdal-Barenblatt model takes the plastic zone as a virtual crack with strip-type tape before a smooth open crack, and it has cohesive stress distribution preventing crack propagation[11]. In the fracture process, the division point of the fracture extension zone and undamaged area is the endpoint of the virtual crack, and the prefabricated crack tip point is the initial point of crack propagation. The distance between the two points is the virtual crack length d. So the total crack length can be written as

$$a = a_0 + d \tag{4}$$

where $0 \leqslant d \leqslant (h - a_0)$. In the fracture process zone (FPZ), the cohesive force existing in the damage area of crack tip nearby can greatly decrease the stress singularity at the crack tip, causing the bearing capacity of the structure to change. Based on the combination of the double-K criterion for the cracking process[7] and the intensity factor calculation of the cohesive resistance stress of FPZ:

$$K_{\mathrm{I}}^{P} = k_0 + K_{\mathrm{I}}^{\sigma} \tag{5}$$

where, K_{I}^{P} is the SIF corresponding the load of remote field, and its superscript refers to the load of remote field; k_0 is the crack-initiated SIF, which is believed to be a constant for the material; and K_{I}^{σ} is the intensity factor of the cohesive stress, and it is related to the thickness and ligament length of specimen. Then:

$$K_{\mathrm{I}}^{\sigma} = \phi \left(\frac{b}{B_0}\right)^{1/2} \left(1 + \frac{d}{h - a_0}\right)^{m} \sqrt{\frac{d}{2\pi}} \tag{6}$$

where, ϕ is a parameter with stress dimension, which is related to the ultimate tensile stress of material; B_0 is the feature thickness; and m is a parameter. Substituting Eqn. (4) into Eqn. (3) and Eqn. (6) into Eqn. (5), and replacing K_{I} in Eqn. (3) with $K_{\mathrm{I}}^{\mathrm{P}}$ in Eqn. (5), Eqn. (7) can be obtained:

$$P = \{2bh^2 [k_0 + \phi (\frac{b}{B_0})^{1/2} (1 + \frac{d}{h - a_0})^{m} \sqrt{\frac{d}{2\pi}}] (1 + 2\frac{a_0 + d}{h}) (1 - \frac{a_0 + d}{h})^{3/2} \} / [3s \sqrt{a_0 + d} \{1.99 - \frac{a_0 + d}{h} (1 - \frac{a_0 + d}{h}) [2.15 - 3.93 (\frac{a_0 + d}{h}) + 2.7 (\frac{a_0 + d}{h})^2]\}] \tag{7}$$

In terms of the formula, the relation curve between load P and crack extension d can be derived, and the peak load of the curve is the estimated value of the ultimate carrying capacity of specimen. As the crack-initiated intensity factor k_0 is almost equivalent to $K_{\mathrm{I}}^{\mathrm{e}}$ in Table 1, it is taken as $k_0 = 54$ MPa · $\mathrm{m}^{1/2}$. Then $\phi = 760$ MPa, $m = 3.5$, and $B_0 = 30$ mm. Through calculation, the values of the estimated ultimate carrying capacities of many specimens are listed in Table 3. The errors between the average value for test maximum load and the peak value of calculated by Eqn. (7), are also listed in Table 3. From this table, the maximum absolute value of the relative error is seen to be 9.61%, i.e. less than 10%. The estimation method for the maximum carrying capacity of a component with a defect by means of fracture mechanics is therefore feasible.

6 Conclusions

1) If the SIF is defined as the limiting load when the elastic zone just reaches the plastic zone for a specimen, then it is a material parameter and independent of the structure size.

2) The fracture toughness arising from the SIF of a specimen at maximum load is affected by size, because its value increases with increasing thickness and ligament length.

3) When a specimen with a prefabricated crack is reloaded after having reached plastic stage, the unloading law applies to it. In other words, when the specimen with crack is loaded into plastic state, the unloading line of relation between loading and its displacement is parallel with the initial elastic line.

4) When an uncracked bending beam of rectangular cross-section is loaded to the elasto-plastic boundary, the value of the Poisson ratio of the plastic zone is about 0.5.

5) For a cracked carbon steel bending beam, the ultimate load capacity can be roughly estimated by combining the SIF of crack resistance and the double-K fracture criterion.

6) Although the fields of deformation and the stress of the crack front in carbon steel are compli-

cated, the results of the digital-optical test show that it is in accord with the predictions of elasto-plastic theory.

References:

[1] Neman Jr J C, James M A, Zerbst U. A Review of the CTOA/CTOD Fracture Criterion [J]. Engineering Fracture Mechanics, 2003, 70(3): 371.

[2] Ahn D C, Sofronis P, Dodds Jr R. Modeling of Hydrogen-Assisted Ductile Crack Propagation in Metals and Alloys [J]. International Journal of Fracture, 2007, 145(2): 135.

[3] Sanda Cleja-Tigoiu. Elasto-Plastic Materials With Lattice Defects Modeled by Second Order Deformations With Non-zero Curvature [J]. International Journal of Fracture, 2010, 166(1): 61.

[4] WEI Yuo-guang, Hutchinsion J W. Steady-State Crack Growth and Work of Fracture for Solids Characterized by Strain Gradient Plasticity [J]. Journal of Mechanics and Physics of Solids, 1997, 45(8): 1253.

[5] Pineau A. Modeling Ductile to Brittle Fracture Transition in Steels—Micromechanical and Physical Challenges [J]. International Journal of Fracture, 2008, 150(1): 129.

[6] Karihaloo B L, Xiao Q Z. Asymptotic Fields at the Tip of a Cohesive Crack [J]. International Journal of Fracture, 2008, 150(1): 55.

[7] XU Shi-lang, Reinhardt H W. Determination of Double-K Criterion for Crack Propagation in Quasi-Brittle Fracture [J]. International Journal of Fracture, 1999, 98(2): 111.

[8] YU Qiang, Le J, Hoover C G, et al. Problems With Hu-Duan Boundary Effect Model and Its Comparison to Size-Shape Effect Law for Quasi-Brittle Fracture [J]. Journal of Engineering Mechanics, 2010, 136(1): 40.

[9] WANG Li-min, XU Shi-lang, ZHAO Xi-qiang. Analysis on Cohesive Crack Opening Displacement Considering the Strain Softening Effect [J]. Science in China G, 2006, 49(1): 88.

[10] Christopher C J, James M N, Patterson E A, et al. Towards a New Model of Crack Tip Stress Fields [J]. International Journal of Fracture, 2007, 148(4): 361.

[11] WANG Li-min, SUN Ming-yuan. Electronical Measurement of Fracture Process of Cast Iron Incision Specimen and Calculation of the Structure Bearing Capacity [J]. Acta Metallurgica Sinica, 2008, 44(7): 853.